The influence of peptide structure on fragmentation pathways

Bari, Sadia

Chapter 4

Fragmentation of α– and β–alanine molecules by ions at Bragg–peak energies

The interaction of keV He$^+$, He^{2+} and O^{5+} ions with isolated α and β isomers of the amino acid alanine was studied by means of high resolution coincidence time–of–flight mass spectrometry. We observed a strong isomer–dependence of characteristic fragmentation channels which manifests in strongly altered branching ratios. Despite the ultrashort initial perturbation by the incoming ion, evidence for molecular rearrangement leading to formation of H_3^+ was found. The measured kinetic energies of ionic alanine fragments can be sufficient to induce secondary damage to DNA in a biological environment.
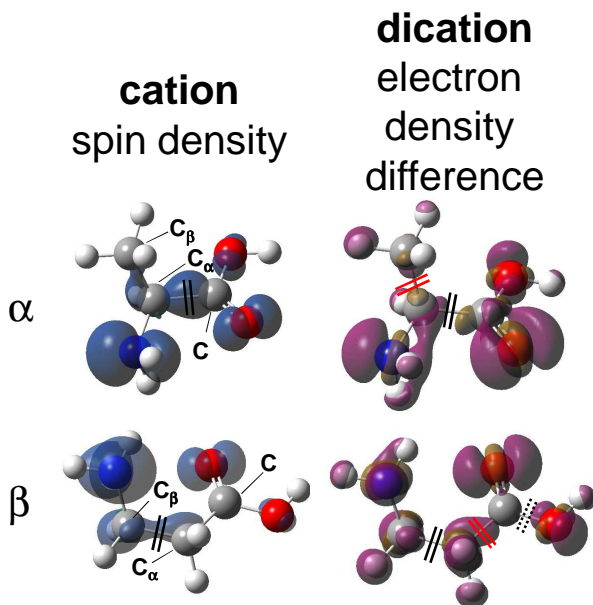
Figure 4.1: *Molecular structure of α– (top) and β–alanine (bottom, red: O, blue: N, light grey: C, white: H). In the left column, the spin density of the cationic molecule is indicated as shaded area, in the right column, the electron density difference map of the dication with respect to the cation is displayed. The double lines indicate bond scission leading to the dominating fragments.*

4.1   Introduction

Biological effects of ionizing radiation are known to be mainly due to direct or indirect damage of cellular DNA. To understand biological radiation damage on a molecular level, a number of recent studies have focused on ionization and fragmentation of isolated DNA building blocks. It was for instance found that very low energy (secondary) electrons can efficiently damage nucleobases [1–3] or deoxyribose [4] and eventually lead to DNA single and double strand breaks [5–7]. The interaction of keV ions with DNA is of major biological relevance in the context of the recent advances in proton and heavy ion tumor therapy. When the ions are decelerated to sub MeV energies, the so–called Bragg–peak is reached where the induced damage is maximum. It has been observed that nucleobases [8–12] and even more so deoxyribose molecules [13] are very sensitive to keV ion impact. Furthermore, secondary ions produced in such collisions can have kinetic energies easily exceeding 10 eV [9, 10] which is sufficient to cause subsequent DNA damage [14, 15].

In the nuclei of eukaryotic cells, DNA is wound around protein spools – the so–called histones. The radiation action upon these proteins is of interest since secondary particles formed during the interaction might in turn damage the neighboring DNA. We have studied the singly and multiply charged ion (MCI) induced ionization and fragmentation of a common protein building–block, the amino acid alanine. Collisions are studied at keV (Bragg–Peak)
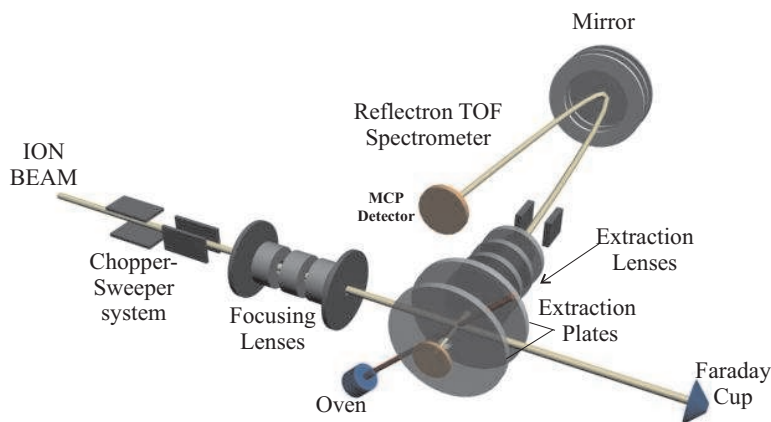
Figure 4.2: *Sketch of the experimental setup.*

projectile energies with emphasis on the determination of secondary ion energies.

Alanine (CH_3–$CH(NH_2)$–$COOH$) is the only amino acid which naturally occurs in two different isomers (α– and β–alanine). The two alanine isomers are depicted in fig. 4.1 with the molecular structure of their lowest energy gas–phase conformer, as experimentally identified by Alonso *et al.* [16, 17]. This availability of two stable isomers allowed us to also address the fundamental question whether there is a structural sensitivity of biomolecular fragmentation pathways following collisions with multiply charged ions. It is known e.g. from MCI collisions with C_{60} that electron capture at large impact parameters can be a very gentle ionization process accompanied by only small amounts of target excitation [18, 19]. Distinct isomer effects in the ionization and fragmentation dynamics following MCI interactions with alanine would indicate fragmentation patterns might also contain structural information for other amino acids and possibly even for peptides or proteins. This could ultimately be interesting for potential application of keV MCI impact as a tool for protein sequencing.

In addition, very recently De *et al.* observed H_3^+ formation in collisions of keV Ar^{8+} ions with methanol molecules [20] – a process which is important e.g. for interstellar gas–phase chemistry. The H_3^+ could only be formed via fast bond rearrangement following Franck–Condon type double ionization processes. In this paper we show that H_3^+ formation following MCI collisions is not limited to methanol but also occurs in both α– and β–alanine and thus seems to be a more general phenomenon.

4.2   Experiment

The experimental setup has been described in detail before [8]. A sketch is displayed in fig. 4.2. Briefly, He^+, He^{2+} and O^{5+} ions were extracted from the electron cyclotron resonance (ECR) ion source located at the ZernikeLEIF facility (KVI in Groningen).

For the present experiments, the source was operated on potentials between 4 and 20 kV. The ion beam was pulsed with a repetition rate in the 10 kHz range and an ion–pulse length of about 10 ns. In the setup, the ion beam was collimated by means of two 1 mm diaphragms (205 mm apart) and focused into the collision region.

In the collision chamber, the ion beam pulses crossed a gaseous target of α– or β–alanine, evaporated from an oven resistively heated to 420 K. This temperature ensured sufficient target densities without thermal dissociation of the molecules. The molecules then effused through a 500 μm nozzle placed $\approx$ 20 mm from the collision region. A liquid nitrogen cooled stainless steel plate opposite to the oven nozzle serves as a trap for the alanine as well as residual gas components. This way the base pressure during experiments is kept around 1×10^{-8} mbar and contributions of the residual gas to the experimental data are negligible.

Two extraction plates located 10 mm apart provide a static electric field. For most experiments, an electric field of 150 V/cm was used. To avoid coverage of these plates by adsorbed layers of alanine, which would distort the homogeneous field, both plates were resistively heated to $\approx$ 100° C. Due to the electric field, ions generated in the collision region were extracted through a diaphragm and a lens system into a reflectron time–of–flight (TOF) spectrometer (resolution $\frac{m}{\Delta m}$ =1500 at m=720 amu [21]) and detected on a multi–channel–plate (MCP) detector. The signal sent to the ion–beam pulser was used as a start for the TOF measurement and for each start, several fragment ions could be detected in coincidence (dead time $\approx$ 50 ns) and analyzed in an event–by–event mode. Electronically, this was accomplished by using a multi–hit time–to–digital converter (TDC, FAST 7888, 1 ns resolution).

4.3   Results and Discussion

A typical mass spectrum of positively charged products from collisions of 40 keV He^{2+} with the two alanine isomers is shown in fig. 4.3. For α–alanine, the probability of non–dissociative ionization is negligible but also for β–alanine, the contribution of the parent cation is weak. For both isomers, the fragmentation spectra are particularly rich and for α–alanine a qualitative resemblance with data obtained after low energy electron impact [22] and core–excitation [23] is obvious. A list with the yields of the most dominant α–alanine fragments and their tentative assignment can be found in table 4.1. Data for He$^+$ and O^{5+} are given for comparison.

One issue to address here is the formation of H$_3^+$ fragment ions. This process has been observed recently for MCI induced double ionization of CH$_3$OH and the H$_3^+$ was confirmed to exclusively stem from the methyl group [20]. We observe H$_3^+$ formation as a weak channel in all collision systems (see inset in fig. 4.3), being strongest for 50 keV O^{5+} projectiles (α–alanine: 0.1% of the H$^+$ ion yield, β–alanine: 0.05%) and about a factor of two smaller for 10 keV He$^+$ and He^{2+} at different kinetic energies. β–alanine does not have a CH$_3$ group and H$_3^+$ formation therefore requires proton migration. α–alanine on the other hand has a CH$_3$ side chain. H$_3^+$ formation in this case does not necessarily require proton migration. However, when using α–alanine with a fully deuterated side chain we observed about twice as much D$_2$H$^+$ as D$_3^+$. Also for α–alanine, the tri–hydrogen cation is therefore primarily formed in a process requiring proton migration.

For α–alanine, the dominant fragment cations are found at $m/q = 1$ (H$^+$) and at m/q=44
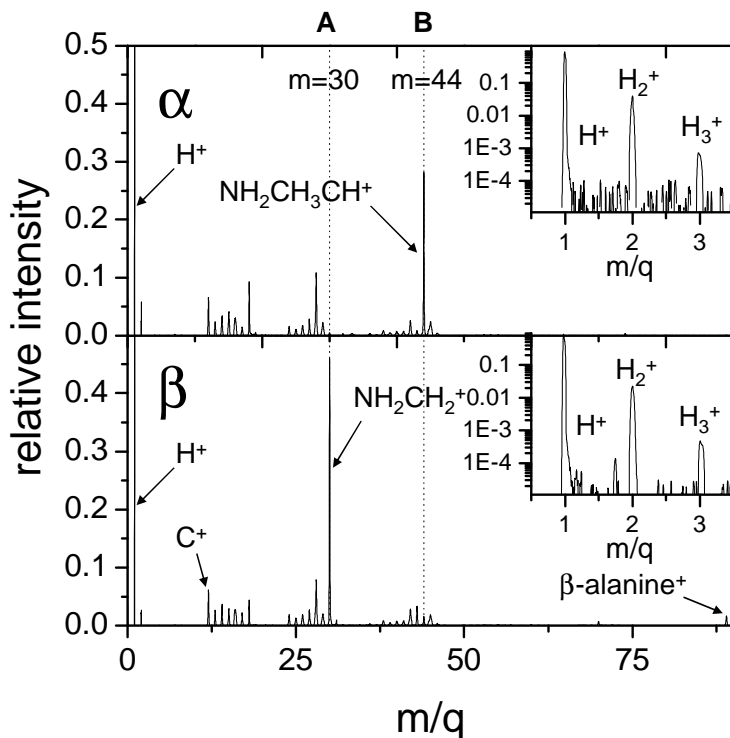
Figure 4.3: *Mass spectrum of product ions from 40 keV He^{2+} collisions with α–alanine (top) and β–alanine (bottom).* **A** *and* **B** *label the main interaction products NH$_2$CH$_2^+$ and NH$_2$CH$_3$CH$^+$, formed by cleavage of the C–C$_\alpha$ bond (α–alanine) and of the C$_\alpha$–C$_\beta$ bond (β–alanine), respectively.*

(NH$_2$CH$_3$CH$^+$, referred to as **B** in fig. 4.3). The latter fragment is formed by a single rupture of the C–C$_\alpha$ bond indicated in fig. 4.1. *Ab initio* calculations on fragmentation channels of the α–alanine cation find this channel to be energetically most favorable [25].

For β–alanine, H$^+$ is again found to dominate the spectrum, together with the fragment at m/q=30 (NH$_2$CH$_2^+$, referred to as **A** in fig. 4.3). The latter fragment is formed by a single rupture of the C$_\alpha$–C$_\beta$ bond indicated in fig. 4.1. Fragment **A** is almost absent for α–alanine whereas fragment **B** is almost absent for β–alanine. Qualitatively the same results are observed for the other projectile ions and ion energies with the exception of He$^+$ projectiles, where channels **A** and **B** are less dominant. Similar findings have been reported for electron impact ionization [26] and for photoionization studies [24].

Compared to these techniques, single electron capture from a molecule by a MCI is very selective i.e. restrained to capture from the highest occupied molecular orbital (HOMO). In the keV energy range single electron capture also is the process with the largest cross–section, dominating the fragmentation pattern in fig. 4.3. As mentioned in the introduction, single electron capture from MCI is furthermore known to be an extremely gentle process,

Table 4.1: *Relative yields of the dominant cationic fragments (yield: 0.1 % or more with the exception of H_3^+) of α–alanine formed in collisions with 10 keV He^+, 20 keV He^{2+} and 50 keV O^{5+}.* [a] *labels fragment ion assignments following the work of Jochims et al. [24].*

m/q (amu)	ion assignment	He^+ (%)	He^{2+} (%)	O^{5+} (%)
1	H^+	32.4	41.9	44.8
2	H_2^+	1.7	0.6	1.6
3	H_3^+	0.07	0.02	0.9
12	C^+	2.5	4.0	5.9
13	CH^+	2.3	2.0	1.3
14	CH_2^+, N^+	4.1	2.8	4.3
15	CH_3^+ [a]	6.9	2.7	3.2
16	NH^+, O^+	3.5	3.5	5.2
17	NH_3^+, OH^+	2.3	1.3	1.7
18	NH_4^+, H_2O^+ [a]	3.4	3.9	3.0
24	C_2^+	0.7	1.2	0.9
25	C_2H^+	1.2	1.0	0.5
26	$C_2H_2^+$	2.5	1.5	1.2
27	$C_2H_3^+$ [a]	3.8	1.7	1.6
28	$HCNH^+$ [a]	10.2	5.9	5.7
29	NH_2CH^+ [a]	3.4	1.7	2.4
30	$NH_2CH_2^+$ [a]	0.3	0.3	0.4
36	C_3^+	0.2	0.3	0.2
37	C_3H^+	0.2	0.2	0.1
38	$C_3H_2^+$, C_2N^+	1.0	0.8	0.5
39	$C_3H_3^+$, C_2NH^+	0.9	0.5	0.5
40	$C_3H_4^+$, $C_2NH_2^+$	1.8	0.7	0.8
41	$C_3H_5^+$, $C_2NH_3^+$	2.1	0.6	0.7
42	$NH_2CH_2C^+$ [a]	3.3	1.4	1.2
42	$NH_2CH_2CH^+$ [a]	0.7	0.5	0.4
44	$NH_2CH_3CH^+$ [a]	3.3	14.1	7.7
45	$COOH^+$ [a]	3.7	2.1	2.7
46	$HCOOH^+$	0.1	0.1	0.1
52		0.1	0.1	0.1
53		0.2	0.1	0.1
54		0.1	0.1	0.1
55	$C_3NH_5^+$	0.1	0.1	0.1
56		0.1	0.1	0.1
75	$NH_2CHCOOH^+$ [a]	<0.1	0.2	0.1

accompanied only by weak excitation of the target molecule [18, 19]. This is stressed by the fact that the isomer specificity of the obtained mass spectra is absent for He^+ impact (see table 4.1, 4.2) which is known to cause most violent fragmentation in biomolecules [9, 13]. For O^{5+} the isomer specificity is weakened due to the fact that gentle single electron capture competes with gentle multi–electron captures, the latter leading to more severe fragmentation.

For a qualitative understanding of the isomer–selective fragmentation pattern, we consider the spatial spin densities of the two alanine radical cations. Overlaid on the lowest energy conformer structures, fig. 4.1 shows the spatial distribution of the α– and β–alanine cation spin–densities, as obtained by density functional theory calculations on the B3LYP level using a 6-311++G(d,p) basis set [27]. Since the interaction time between ions and amino

Table 4.2: *Relative yields of the dominant cationic fragments (yield: 0.1 % or more with the exception of H_3^+) of β–alanine formed in collisions with 10 keV He^+, 20 keV He^{2+} and 50 keV O^{5+}. [a] labels fragment ion assignments following the work of Jochims et al. [24].*

m/q (amu)	fragment ion	He^+ (%)	He^{2+} (%)	O^{5+} (%)
1	H^+	27.5	38.3	37.5
2	H_2^+	1.3	1.1	1.2
3	H_3^+	0.03	0.02	0.05
12	C^+	2.2	3.7	6.0
13	CH^+	2.3	1.7	14
14	CH^+, N^+	4.1	2.7	4.4
15	CH_3^+ [a]	4.2	1.7	1.7
16	NH^+, O^+	3.5	3.8	5.3
17	NH_3^+, OH^+	2.5	1.6	2.0
18	NH_4^+, H_2O^+ [a]	1.7	1.5	1.4
19	H_3O^+	0.3	0.1	0.2
24	C_2^+	1.0	1.5	1.1
25	C_2H^+	1.6	1.2	0.7
26	$C_2H_2^+$, CN_+	2.8	1.6	1.5
27	$C_2H_3^+$ [a]	4.2	1.9	1.9
28	$HCNH^+$ [a]	10.6	5.5	6.1
29	NH_2CH^+ [a]	3.4	1.8	2.6
30	$NH_2CH_2^+$ [a]	6.6	18.5	12.3
31		0.5	0.3	0.3
37	C_3H^+	0.5	0.1	0.2
38	$C_3H_2^+$, C_2N^+	1.2	0.7	0.6
39		1.1	0.4	0.6
40		1.9	0.6	0.9
41		2.4	0.7	1.0
42	$NH_2CH_2 = C^{\bullet +}$ [a], CH_2CO^+	4.3	1.8	2.2
43	$NH_2CHCH_2^+$ [a]	1.3	1.5	1.2
44	$NH_2(CH_2)_2^+$ [a]	1.2	1.1	1.1
45	$COOH^+$ [a]	3.5	1.7	2.5
46			0.2	0.3
50		0.2		
51		0.1		
52		0.2	0.1	0.1
53		0.3	0.1	0.1
55		0.1	0.1	0.1
60	CH_3COOH^+ [a]		0.1	0.1
70	$NH_2CHCHCO^+$ [a]		0.3	0.2
89	$NH_2(CH_2)_2COOH^+$	0.1	0.7	0.6

acids is on the fs time–scale, we assumed a vertical ionization. The geometries have thus been optimized for the neutral molecules. In agreement with the study of Simon *et al.* [25] the spin density for α–alanine is centered around the NH_2 (amino) group. We find similar results for β–alanine. In both cases, weaker contributions of spin density are also found on the respective COOH groups. However, for α–alanine where the amino–group is bound to the central C atom, the ionization substantially weakens the C–C_α bond whereas for β–alanine
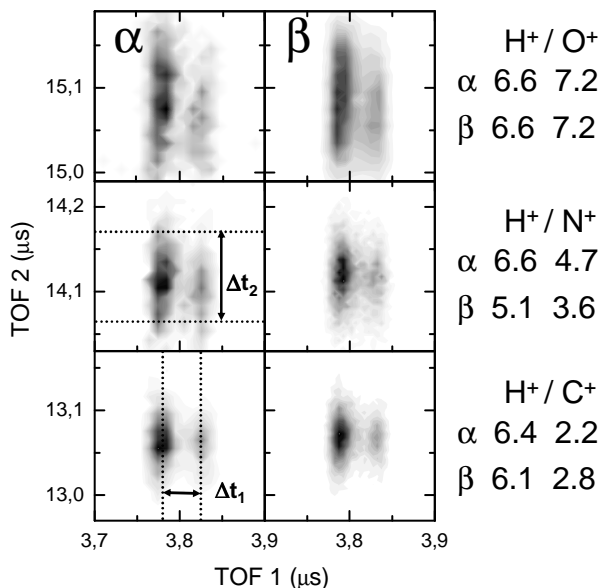
Figure 4.4: *Correlation plot for H^+/C^+, H^+/N^+ and H^+/O^+ ion pairs from 40 keV He^{2+} collisions with α– and β–alanine. On the right, kinetic energies are given for each fragment ion in eV (see text).*

the C_α–C_β bond is weakened (see fig. 4.1). This is in agreement with the experimental data in which scission of these bonds is preferentially observed.

Fragmentation patterns as the ones shown in fig. 4.3 mostly contain information on possible endpoints of the ion–induced dissociation processes as well as on their respective branching ratios. When only examining those ionization processes in which the alanine molecules are at least doubly ionized, two or more fragment cations stemming from the same molecular fragmentation event can be detected in coincidence and more in depth information on the fragmentation dynamics can be obtained. In the following, we will focus on the analysis of those fragmentation channels that involve the most abundant fragment ions from fig. 4.3, i.e. $NH_2CH_3CH^+$ (α–alanine), $NH_2CH_2^+$ (β–alanine) and H^+ (both).

Fragment–fragment correlations involving protons are dominating the correlation diagrams for both isomers. Furthermore, protons are often the most energetic secondary ions observed in ion–induced biomolecular fragmentation [9]. Fig. 4.4 exemplarily displays the correlation plots for H^+ (TOF1) with C^+, N^+ and O^+ (TOF2) formed after multiple ionization of α– and β–alanine by 40 keV He^{2+} ion impact. Note that the double–island structure is due to the transmission of the extraction system. In the collision center fragment ions with a specific kinetic energy are produced. The static electric extraction field applied to the collision region accelerated the ions towards a diaphragm of finite diameter. Depending on the diaphragm diameter, its distance from the collision center and the strength of the extraction field, a cutoff ion energy exists. Ions with kinetic energies exceeding this cutoff energy have transmissions smaller than 100 %. For a single ion the transmission depends on the ions mo-
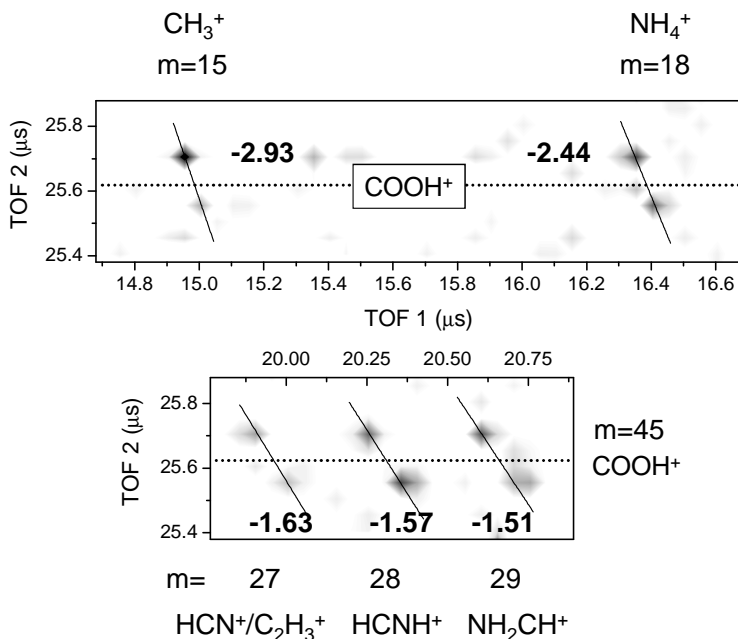
CH$_3^+$
m=15

NH$_4^+$
m=18

TOF 2 (µs)

25.8

-2.93

-2.44

COOH$^+$

25.6

25.4

14.8 15.0 15.2 15.4 15.6 15.8 16.0 16.2 16.4 16.6

TOF 1 (µs)

20.00 20.25 20.50 20.75

TOF 2 (µs)

25.8

25.6

m=45
COOH$^+$

25.4

-1.63 -1.57 -1.51

m= 27 28 29

HCN$^+$/C$_2$H$_3^+$ HCNH$^+$ NH$_2$CH$^+$

Figure 4.5: *Correlation plot for fragment ions from 40 keV He^{2+} collisions with α–alanine with intensities given in logarithmic scale. Only the regions corresponding to m/q=15–18 and m/q=27-29 coincidences with COOH$^+$ are shown, with the number indicating the respective island slope.*

mentum vector. If the angle between ion momentum and detector axis is 90° the ion will reach the diaphragm at maximum distance from the center. If this angle is zero, the ion will reach the diaphragm at the diaphragm center. For fragment ions with kinetic energies exceeding the cutoff, therefore only the ones emitted parallel or antiparallel to the spectrometer axis are detected. In case of 100 % transmission, parallelogram–shaped islands would be observed. In fig. 4.4 for the protons a structure with two maxima is observed and Δt_1 is defined as the distance between these maxima. For the heavy ions, no double peak structure is observed. As a measure for their kinetic energies we use the time (Δt_2) between those TOFs at which the peak intensity dropped to 10 %. For a given extraction field ε, fragment charge state q and fragment ion mass m the ion kinetic energy is given by $E = \varepsilon^2 q^2 \Delta t^2 / 8m$. The determined energies for fragments of α– and β–alanine are given on the right of fig. 4.4 (in eV).

It is obvious that the fragment ion kinetic energies depend strongly on the fragment ion type, being largest for O$^+$ and H$^+$ and smallest for C$^+$. The isomer dependence is relatively weak. For O^{5+} projectiles qualitatively the same trends are observed but since on average fragmentation involves higher initial alanine charge states, fragment kinetic energies exceed 15 eV (H$^+$, most probable energy) and 17 eV (O$^+$, energy at 10 % cutoff). On the other hand, for He$^+$ ions for which resonant electron capture is unlikely [8] a strong isomer dependence is observed.

In case of double ionization of α–alanine, the dominating large fragment NH$_2$CH$_3$CH$^+$

formed by scission of the C–C$_\alpha$ bond is not seen as a strong fragmentation channel in the correlation data. Apparently, two electron removal quenches this fragment and leads to more extensive fragmentation of this ion. Somewhat weak but as the most intense feature at larger fragment masses, we observe the corresponding COOH$^+$ fragment at $m/q = 45$ which is only a minor channel in single ionization (see table 4.1). The relevant parts of the respective correlation plots are displayed in fig. 4.5. The COOH$^+$ ion is observed strongest in coincidence with the NH$_2$CH$^+$ ion ($m/q = 29$) and to a weaker extent with HCNH$^+$ ($m/q = 28$) and HCN$^+$ ($m/q = 27$), note that Jochims $et\ al.$ [24] assign this m/q to C$_2$H$_3^+$. Our results indicate that the three m/q differ in hydrogen content favoring the HCN$^+$ assignment. A second group of islands represent coincidences of COOH$^+$ with CH$_3^+$ ($m/q = 15$) and NH$_4^+$ ($m/q = 18$).

The slope of islands in TOF/TOF correlation plots carries information on the momentum balance of the respective fragment ions. If the two ions stem from a two–body breakup, conservation of momentum implies a -1 slope of the respective island in the correlation plot. Non–conservation of mass obviously rules out two body breakup and a two–step process has to be invoked.
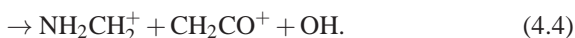
In fig. 4.5 the islands have a much steeper slope indicating a secondary decay mechanism [28] subsequent to the first step in which the C–C$_\alpha$ bond is broken. In the second step, the NH$_2$CH$_3$CH$^+$ ion fragments e.g. along the C$_\alpha$–C$_\beta$ bond (pair (45,29)) according to the following scheme:

$$\text{NH}_2\text{CH}_2\text{CH}_2\text{COOH}^{++} \rightarrow \text{NH}_2\text{CH}_3\text{CH}^+ + \text{COOH}^+ \qquad (4.1)$$
$$\rightarrow \text{NH}_2\text{CH}^+ + \text{CH}_3 + \text{COOH}^+ \qquad (4.2)$$

If no kinetic energy is released in the second step, then the NH$_2$CH$^+$ cation leaves with the same velocity as the initial NH$_2$CH$_3$CH$^+$ cation. The slope of the island has to be -m(NH$_2$CH$_3$CH$^+$)/m(NH$_2$CH$^+$)=-44/29=-1.51, which is in line with the experimental data (see fig. 4.5). A similar fragmentation sequence leads to the pairs (45,28) (slope=-1.57) and (45,27) (slope=-1.63) in which either one or two hydrogen atoms are lost in the second step. In case the charge stays on the smaller CH$_3$ fragment, the pair (45,15) (slope=-2.93) is observed. The last channel seen in fig. 4.5 corresponding to the pair (45,18) (slope=-2.44) leads to formation of an NH$_4^+$ ion. This channel involves rearrangement of the NH$_2$CH$_3$CH$^+$ cation [26].

The kinetic energy release in step 1 amounts to 2.2±0.2 eV (pair (30,45)). In the single–stop spectra (fig. 4.3) the dominating fragment cation for β–alanine is NH$_2$CH$_2^+$ (m/q=30). In the coincidence spectra (fig. 4.6), the strongest correlation of m/q=30 is with m/q=42 (CH$_2$CO$^+$). Loss of one or two H atoms from NH$_2$CH$_2^+$ leads to the pairs (29,42) and (28,42). All these islands have a slope very close to -1.

The three pairs (28,42), (29,42) and (30,42) are obviously not the result of a pure 2–body breakup, because a neutral OH fragment is produced in addition. Since two–body breakup is ruled out the -1 slope is an indication for so–called deferred charge separation [28], i.e. loss of a neutral fragment without appreciable energy release (eq. 4.3) and subsequent fragmentation of the remaining dication under conservation of momentum (eq. 4.4):
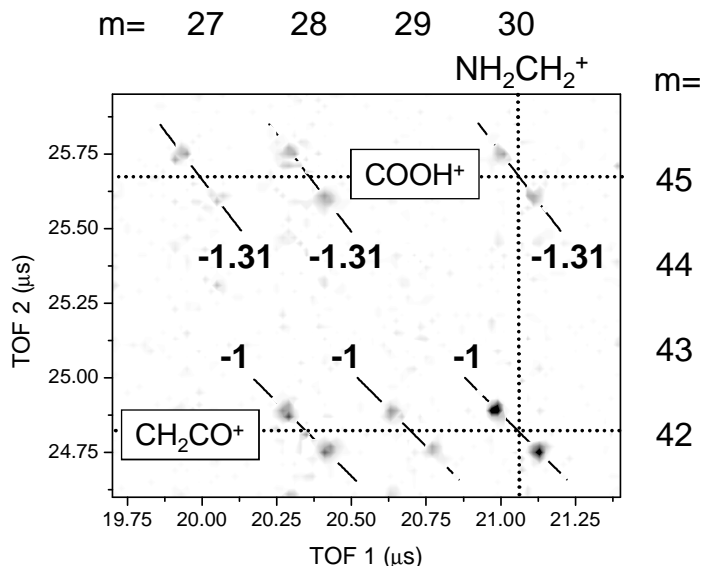
$$\text{NH}_2\text{CH}_2\text{CH}_2\text{COOH}^{++} \rightarrow \text{NH}_2\text{CH}_2\text{CH}_2\text{CO}^{++} + \text{OH}, \qquad (4.3)$$
$$\rightarrow \text{NH}_2\text{CH}_2^+ + \text{CH}_2\text{CO}^+ + \text{OH}. \qquad (4.4)$$

Figure 4.6: *Correlation plot for fragment ions from 40 keV He^{2+} collisions with β–alanine with intensities given in logarithmic scale. Only the region corresponding to NH$_2$CH$_2^+$ (-H$_n$) (due to cleavage of the C$_\alpha$–C$_\beta$ bond) coincidences with COOH$^+$ (due to cleavage of the C–C$_\alpha$ bond) and CH$_2$CO$^+$ (due to cleavage of the C–O single bond) are shown, with the number indicating the respective island slope.*

The kinetic energy released in the second step can be obtained from the Δt of the respective island and amounts to 3.5$\pm$0.2 eV for the fragmention into the pair (30,42). A weaker group of islands involving the most prominent NH$_2$CH$_2^+$ (m/q=30) cation is due to correlations with m/q=45 (COOH$^+$). This channel is also observed accompanied by loss of 2 or 3 H atoms from the lighter fragment, leading to pairs (28,45) and (27,45). Here, the islands have a much steeper slope indicating a secondary decay mechanism [28].

$$NH_2CH_2CH_2COOH^{++} \rightarrow NH_2CH_2^+ + CH_2COOH^+ \tag{4.5}$$
$$\rightarrow NH_2CH_2^+ + COOH^+ + CH_2 \tag{4.6}$$
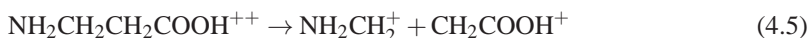
Again, if no kinetic energy is released in the second step, then the COOH$^+$ cation leaves with the same velocity as the initial CH$_2$COOH$^+$ cation. The slope of the islands has to be -m(CH$_2$COOH)/m(COOH)=-59/45=-1.31, which agrees very well with what is observed in fig. 4.6. The kinetic energy release in step 1 amounts to 2.2$\pm$0.2 eV (pair (30,45)). This value is clearly smaller than the 3.5 eV observed for the competing process. The reason might be that the charge separation occurs in the first step, i.e. from the intact molecule. In the deferred charged separation process, the intact molecule has already lost an OH group. Coulomb explosion than occurs in a smaller system where the distances are smaller and Coulomb repulsion is accordingly stronger.

The fragmentation dynamics following alanine double ionization can be interpreted by looking at the electron density difference maps for dications and cations (see fig. 4.1). The

major bond scission following single ionization is marked by black lines. Subsequent bond scissions in the case of double ionization are marked by red lines.

For α–alanine the main fragmentation process after single ionization is scission of the C–C$_\alpha$ bond leading to a neutral COOH fragment. This is also the most common first step after double ionization (see eq. 4.2) with the only difference of COOH being formed in cationic form. From fig. 4.1 this can be expected, since substantial charge is removed from the COOH group upon the 2nd ionization. Furthermore, the CH$_3$ group is again only weakly affected by removal of the second electron. It is this group, which is set free in the second step, either neutral or in cationic form.

Formation of the COOH$^+$ cation is also an important channel in double ionization of β–alanine (see eq. 4.6). It is obvious from the electron density difference maps in fig. 4.1 electron removal from the β–alanine cation changes the electron density throughout the whole molecule. In particular, the C–C$_\alpha$ bond is affected and in case of the C–C$_\alpha$ bond scission, the COOH$^+$ is released in the second fragmentation step.

A peculiarity of the β–isomer is the OH–loss channel (eq. 4.4) which is stronger than the COOH$^+$ production. Here, the *first* step is the scission of the C–O single bond (indicated by dotted lines in fig. 4.1) followed by scission of the C$_\alpha$–C$_\beta$ bond. This process is probably facilitated by a stronger intramolecular hydrogen bonding between the NH$_2$ group and the second O atom.

4.4   Conclusion

To conclude we have observed a pronounced isomer dependence in MCI induced fragmentation of isolated alanine molecules. These results are interesting for future studies on MCI induced protein fragmentation with the ultimate goal of developing a new complementary tool for protein structure determination. Fragment ion kinetic energies were found to exceed 6 eV (He^{2+} impact) and 15 eV (O^{5+} impact) implying that ion–induced damage of histone proteins might produce sufficiently energetic secondary ions to induce further damage to neighboring DNA. Formation of H$_3^+$ ions from both α– and β–alanine was observed. This relatively weak process requires substantial rearrangement of the molecule before fragmentation. Thus, formation of H$_3^+$ cations in MCI induced fragmentation, as first observed by De *et al.* [20], seems to be a more general phenomenon, which is also observed in biomolecular fragmentation.

References

[1] M. A. Huels, I. Hahndorf, E. Illenberger, and L. Sanche, J. Chem. Phys. **108**, 1309 (1998).

[2] H. Abdoul-Carime, M. A. Huels, F. Brüning, E. Illenberger, and L. Sanche, J. Chem. Phys. **113**, 2517 (2000).

[3] G. Hanel, B. Gstir, S. Denifl, P. S. and M. Probst, B. Farizon, M. Farizon, E. Illenberger, and T. D. Märk, Phys. Rev. Lett. **90**, 188104 (2003).

[4] S. Ptasinska, S. Denifl, P. Scheier, and T. D. Märk, J. Chem. Phys. **120**, 8505 (2004).

[5] B. Boudaïffa, P. Cloutier, D. Hunting, M. A. Huels, and L. Sanche, Science **287**, 1658 (2000).

[6] X. Pan, C. Cloutier, D. Hunting, and L. Sanche, Phys. Rev. Lett. **90**, 208102 (2003).

[7] F. Martin, P. D. Burrow, Z. Cai, P. Cloutier, D. Hunting, and L. Sanche, Phys. Rev. Lett. **93**, 068101 (2004).

[8] J. de Vries, R. Hoekstra, R. Morgenstern, and T. Schlathölter, J. Phys. B **35**, 4373 (2002).

[9] J. de Vries, R. Hoekstra, and R. M. and T. Schlathölter, Eur. Phys. J. D **24**, 161 (2003).

[10] J. de Vries, R. Hoekstra, R. Morgenstern, and T. Schlathölter, Phys. Rev. Lett. **91**, 053401 (2003).

[11] R. Brédy, J. Bernard, L. Chen, B.Wei, A. Salmoun, T. Bouchama, M. Buchet-Poulizac, and S. Martin, Nucl. Instrum. Meth. B **235**, 392 (2005).

[12] T. Schlathölter, F. Alvarado, S. Bari, A. Lecointre, R. Hoekstra, V. Bernigaud, B. Manil, J. Rangama, and B. Huber, ChemPhysChem **7**, 2339 (2006).

[13] F. Alvarado, S. Bari, R. Hoekstra, and T. Schlathölter, Phys. Chem. Chem. Phys **8**, 1922 (2006).

[14] Z. Deng, I. Bald, E. Illenberger, and M. A. Huels, Phys. Rev. Lett. **95**, 153201 (2005).

[15] Z. Deng, I. Bald, E. Illenberger, and M. A. Huels, Phys. Rev. Lett. **96**, 243203 (2006).

[16] S. Blanco, A. Lesarri, J. C. Lopez, and J. L. Alonso, J. Am. Chem. Soc. **126**, 11675 (2004).

[17] M. E. Sanz, A. Lesarri, M. I. Pena, V. Vaquero, V. Cortijo, J. C. Lopez, and J. L. Alonso, J. Am. Chem. Soc. **128**, 3812 (2006).

[18] B. Walch, C. L. Cocke, R. Voelpel, and E. Salzborn, Phys. Rev. Lett. **72**, 1439 (1994).

[19] T. Schlathölter, O. Hadjar, R. Hoekstra, and R. Morgenstern, Appl. Phys. A **72**, 281 (2001).

[20] S. De, J. Rajput, A. Roy, P. N. Ghosh, and C. P. Safvan, Phys. Rev. Lett. **97**, 213201 (2006).

[21] O. Hadjar, R. Hoekstra, R. Morgenstern, and T. Schlathölter, Phys. Rev. A **63**, 033201 (2001).

[22] I. Ipolyi, P. Cicmand, S. Denifl, V. Matejcik, P. Mach, J. Urban, P. Scheier, T. D. Märk, and S. Matejcik, Int. J. Mass Spectr. **252**, 228 (2006).

[23] M. Morita, M. Mori, T. Sunami, H. Yoshida, and A. Hiraya, Chem. Phys. Lett. **417**, 246 (2006).

[24] H.-W. Jochims, M. Schwell, J.-L. Chotin, M. Clemino, F. Dulieu, H. Baumgärtel, and S. Leach, Chem. Phys. **298**, 279 (2004).

[25] S. Simon, A. Gilb, M. Sodupeb, and J. Bertran, Journal of Molecular Structure: THEOCHEM **727**, 191 (2005).

[26] G. Junk and H. Svec, J. Am. Chem. Soc. **85**, 839 (1963).

[27] M. J. Frisch, G. W. Trucks, H. B. Schlegel, G. E. Scuseria, M. A. Robb, J. R. Cheeseman, J. A. Montgomery, Jr., T. Vreven, K. N. Kudin, J. C. Burant, J. M. Millam, S. S. Iyengar, J. Tomasi, V. Barone, B. Mennucci, M. Cossi, G. Scalmani, N. Rega, G. A. Petersson, H. Nakatsuji, M. Hada, M. Ehara, K. Toyota, R. Fukuda, J. Hasegawa, M. Ishida, T. Nakajima, Y. Honda, O. Kitao, H. Nakai, M. Klene, X. Li, J. E. Knox, H. P. Hratchian, J. B. Cross, V. Bakken, C. Adamo, J. Jaramillo, R. Gomperts, R. E. Stratmann, O. Yazyev, A. J. Austin, R. Cammi, C. Pomelli, J. W. Ochterski, P. Y. Ayala, K. Morokuma, G. A. Voth, P. Salvador, J. J. Dannenberg, V. G. Zakrzewski, S. Dapprich, A. D. Daniels, M. C. Strain, O. Farkas, D. K. Malick, A. D. Rabuck, K. Raghavachari, J. B. Foresman, J. V. Ortiz, Q. Cui, A. G. Baboul, S. Clifford, J. Cioslowski, B. B. Stefanov, G. Liu, A. Liashenko, P. Piskorz, I. Komaromi, R. L. Martin, D. J. Fox, T. Keith, M. A. Al-Laham, C. Y. Peng, A. Nanayakkara, M. Challacombe, P. M. W. Gill, B. Johnson, W. Chen, M. W. Wong, C. Gonzalez, and J. A. Pople, Gaussian 03, Revision C.02, Gaussian, Inc., Wallingford, CT, 2004.

[28] J. H. D. Eland, F. S. Wort, and R. N. Royds, J. El. Spectr. Rel. Phen. **41**, 297 (1986).